AAS 03-568

USING BATTIN'S METHOD TO OBTAIN MULTIPLE-REVOLUTION LAMBERT'S SOLUTIONS

Haijun Shen* and Panagiotis Tsiotras†

Abstract

In this paper, Battin's method for the Lambert's problem is extended to calculate the multiple-revolution Lambert's solutions. It is shown that the original successive substitution method described in Battin's method converges to one of the two N-revolution solution with $N \geq 1$. If the order of the original successive substitution is reversed, then the reversed successive substitution converges to the other N-revolution solution. It is also shown that the original successive substitution converges to the N-revolution transfer orbit with the smaller semi-major axis, and the reversed successive substitution converges to the one with the larger semi-major axis. A preprocessing algorithm is given to provide initial guesses with with the convergence of the successive substitution methods is guaranteed.

INTRODUCTION

Lambert's problem deals with the determination of an Keplerian orbit connecting two points in space with a given time-of-flight and the direction of flight. Over the years, different algorithms have been proposed to solve the Lambert's problem. The most notable ones are Gauss' method,[1] the method by Herrick and Liu,[2] Battin's method,[3] etc. A comprehensive analysis along with a collection of historic references are provided in Battin.[4]

This work is motivated by the works of Prussing[5] on Multiple-revolution solutions to the Lambert's problem and Battin[3] on the elegant formulation and algorithm to solve the Lambert's problem. In Ref. 5, a clear analysis of the multiple-revolution solutions to the Lambert's problem based on the classical Lagrange's formulation is presented. Therein, it is shown that for an impulsive circle-to-circle orbital transfer, allowing the spacecraft to stay on the transfer orbit for one or more revolutions could potentially reduce the total fuel consumption of the orbital transfer. It also shows that for a given Lambert's problem, there are two N-revolution transfer orbit with $N > 0$, and there is only one 0-revolution transfer orbit. Therefore, there are a total of $2N_{\max} + 1$ solutions for a given Lambert's problem, with $N_{\max}$ being the maximum number of revolutions allowed. In Ref. 5, the Newton-Raphson iteration scheme is used to solve for the $2N_{\max} + 1$ solutions. However, the convergence

*Senior Project Engineer, Analytical Mechanics Associates, Inc.. Tel: (757) 865-0944, ext. 203, Fax: (757) 865-1881. Email: shen@ama-inc.com.

†Associate Professor, School of Aerospace Engineering, Georgia Institute of Technology. Tel: (404) 894-9526, Fax: (404) 894-2760, Email: p.tsiotras@ae.gatech.edu.

of the Newton-Raphson iteration strongly depends on the initial guesses, and it is not suitable for automated on-line calculations.

In Ref. 3, Battin presented an elegant formulation for the Lambert's problem based on the geometric orbital transformation described in Ref. 6. Battin's formulation resembles the elegance of the Gauss' formulation,[4] but have great advantages over Gauss' formulation. First, the singularity when the transfer angle is π is moved to 2π, which allows Battin's formulation to be suitable for a larger range of problems than Gauss' formulation. In addition, the convergence property of Battin's formulation is better than Gauss' formulation, especially when θ is large, in the sense that Battin's formulation has fewer iterations and convergence is obtained for a larger range of problems. However, the algorithm in Ref. 3 does not yields solutions to Lambert's problem with multiple revolutions.

It is the intent of this paper to extend the algorithm in Ref. 3 to calculate the $2N_{\max}+1$ multiple-revolution transfer orbits. It will be shown that the convergence of the new algorithm does not depend on the choice of initial guesses.

This paper is organized in the following fashion. The multiple-revolution Lambert's problem is introduced first, followed by a brief introduction of Battin's formulation. Then, we present Battin's formulation considering multiple revolutions, and the original successive substitution and the reversed successive substitution methods to obtain the solutions to Battin's formulation. In the end, we establish the correspondence between the two N-revolution transfer orbits and the solutions obtained for Battin's formulation.

MULTIPLE-REVOLUTION LAMBERT'S PROBLEM

A Lambert's problem is stated as the following:[1] given two point P_1 and P_2 in space, the time-of-flight t_f, and direction of flight, determine the Keplerian orbit that takes a body from P_1 to P_2 in the given t_f. Figure 1 illustrates the geometry of a typical Lambert's problem. In the figure, P_1 and P_2 are two fixed points in the space, with radii of r_1 and r_2, F is the primary focus, F^* is the fictitious focus, d stands for the distance between P_1 and P_2, and θ is the transfer angle. The problem is to determine the Keplerian orbit such that a body is at P_1 initially and must arrive at P_2 at a specified time which is denoted by t_f.

An N-revolution transfer orbit is an elliptical orbit passing P_1 and P_2 such that within the given t_f the body travels along the ellipse for N complete revolutions before arriving at P_2. Clearly, the 0-revolution transfer orbit consists of only the portion of the transfer orbit from P_1 to P_2. It should be pointed out that a 0-revolution transfer orbit is not limited to a portion of an ellipse, but can be a portion of any conic.

According to Lambert's theory,[4] the time-of-flight is a function only of the semi-major axis a of the transfer orbit, the sum of the radii r_1+r_2, and the chord length d, i.e.,

$$t_f = f(a,\, d,\, r_1+r_2). \tag{1}$$

For a given Lambert's problem, since r_1+r_2 and d are given, t_f is a function only of the semi-major axis a. The task of finding the transfer orbits is then to determine the semi-major axis a from Eq. (1).

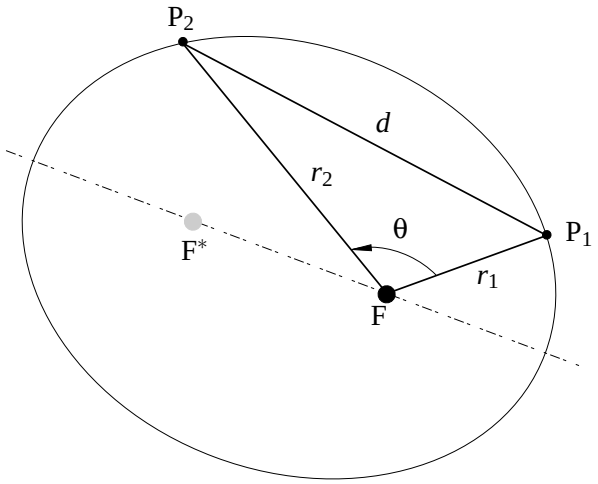

Figure 1: Geometry of the Lambert's problem.

In the following, distance and time are non-dimensionalized. Specifically, distance is normalized by r_1, and time is normalized by the period of a circular orbit with radius of r_1. Hence, under such a unit system, the gravitational parameter $\mu = 4\pi^2$.

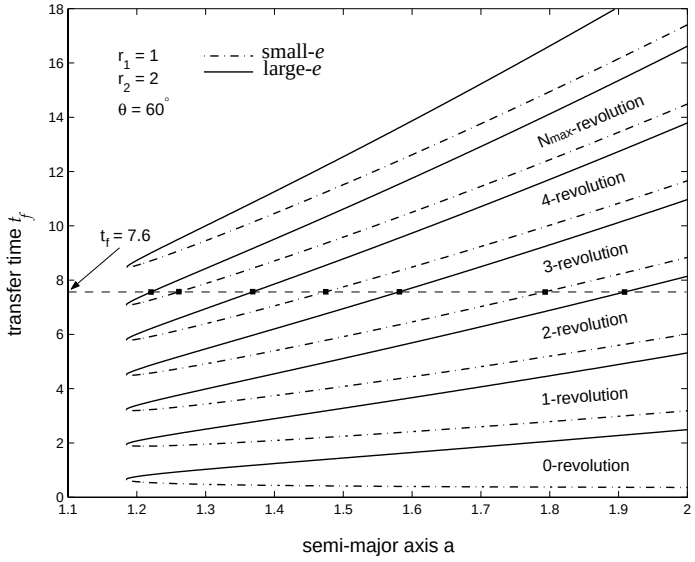

Figure 2: An example plot of t_f vs. a.

It has been shown in Refs. 5 and 7 that, in general, there are more than one transfer orbits for a given Lambert's problem, if multiple revolutions along the transfer orbit are allowed. An example plot of t_f vs. semi-major axis a is shown in Figure 2. This plot corresponds to the case where $r_1 = 1$, $r_2 = 2$, and $\theta = 60^\circ$. In Figure 2, it can be seen that for each N, the number of revolutions, two solution branches exist, an upper branch and a lower branch. For cases where $\theta \leq 180^\circ$, the upper branch corresponds to large-e transfer orbits, and the lower branch corresponds to small-e

transfer orbits. For cases where $\theta \geq 180^\circ$, the upper branch corresponds to small-*e* transfer orbits, and the lower branch corresponds to large-*e* transfer orbits.[8] In Ref. 8, a large-*e* transfer orbit is defined as the one whose two foci lie in the opposite sides of the P_1P_2 line segment, and a small-*e* transfer orbit is defined as the one whose two foci lie in the same side of the P_1P_2 line segment.

It is evident in Figure 2 that for each $N \geq 1$ there are two semi-major axes corresponding to one t_f, determining two N-revolution transfer orbits. As shown in Ref. 8, these two transfer orbits could be two large-*e* transfer orbits, two small-*e* transfer orbits, or one large-*e* and one small-*e* transfer orbits, depending on the transfer angle θ and t_f. However, for $N = 0$, the lower branch monotonically decreases, and the upper branch monotonically increases. Therefore, there is only one semi-major axis corresponding to one t_f, determining either a small-*e* or a large-*e* transfer orbit, depending on the transfer angle θ and t_f. In addition, for any given t_f, there is a maximum number of possible revolutions. Let this maximum number of possible revolutions be denoted by $N_{\max}$. Then, for a given t_f, there are $2N_{\max}+1$ solutions for the multiple-revolution Lambert's problem. For example, in Figure 2, it is shown that for a time-of-flight of $t_f = 7.6$ we have $N_{\max} = 5$. It is clear that there is a total of eleven semi-major axes that determine eleven different transfer orbits connecting P_1 and P_2. Details on how to determine $N_{\max}$ and other characteristics of the t_f vs. a plot can be found in Refs. 5 and 8.

The Newton-Raphson iteration method was used in Ref. 5 and Ref. 7 to calculate the $2N_{\max}+1$ semi-major axes of the transfer orbits. However, convergence of the Newton-Raphson method depends strongly on the initial guesses. In some problems, the convergence can not be guaranteed.[8]

In situations where the Newton-Raphson iteration does not yield the solution, an alternative method must be used. A well-known method for solving Lambert's problem is the one proposed by Battin in Ref. 3. Battin's method was motivated by Gauss' original formulation of the problem. The formulation by Gauss was designed to deal with problems with small transfer angles and possesses a singularity when the transfer angle is π. In Battin's formulation, the singularity at $\theta = \pi$ is moved to $\theta = 2\pi$, so the algorithm is suitable for a large range of transfer angles. In addition, Battin's algorithm has a much faster convergence rate than Gauss' method. However, the original method of Battin is used to solve transfer orbits without considering revolutions. In this paper, we extend it to accommodate the multiple-revolution transfer orbits.

BATTIN'S FORMULATION

The orbit transformation described in Ref. 6 is the basis for Battin's formulation. According to Lambert's theorem,[4] if P_1 and P_2 are held fixed, the primary and fictitious foci F and F^* can be moved without affecting the time-of-flight, provided that $r_1 + r_2$ and the semi-major axis a are unchanged in the process. Doing so, the shape of the transfer orbit will be changed. For the purpose of the new formulation, the transformed orbit is such that its major axis is perpendicular to the line segment P_1P_2.

One example of a transformed elliptical orbit is shown in Figure 3. In this example, the arc along the transformed orbit from P_1 to P_2 passes the periapsis. In the figure, $\eta = (r_1+r_2)/2$, F_0 and F_0^* are the two foci of the transformed orbit, ν denotes the true anomaly of P_2 in the transformed orbit, E denotes the eccentric anomaly of P_2 in the transformed orbit, and r_{0p} denotes the pericenter radius of the parabolic orbit connecting P_1 and P_2. In the transformed orbit, P_1 and P_2 have the

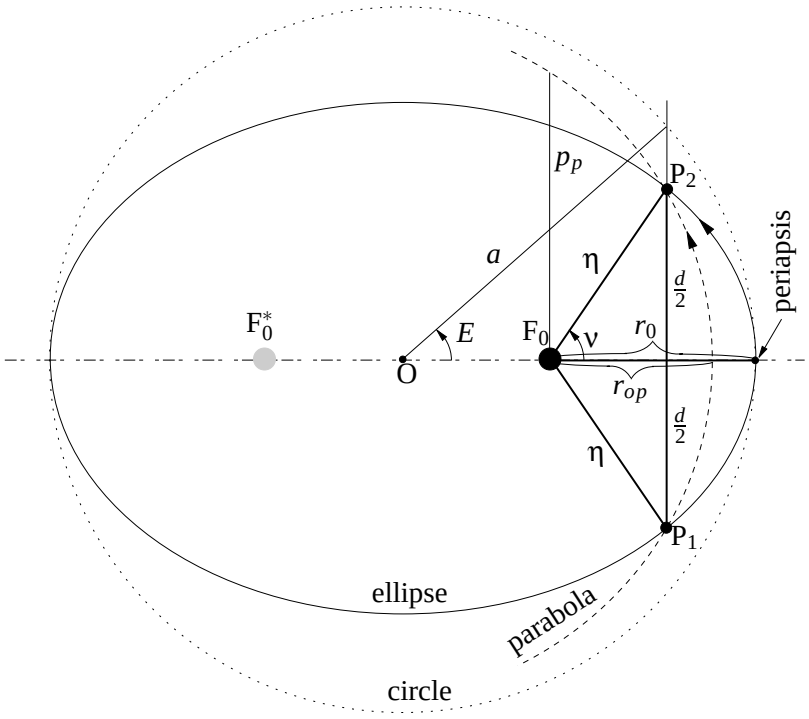

Figure 3: Transformation of the Lambert's problem - the P_1P_2 arc along the transformed orbit passes the periapsis.

same radius which is η, and the radius of the periapsis is r_0. It can be shown[4] that the true anomaly ν of P_2 on the transformed orbit is related to the original transfer angle θ by the following equation.

$$\cos\nu = \frac{\pm\sqrt{\eta^2 - \left(\frac{d}{2}\right)^2}}{\eta} = \frac{\pm\sqrt{s(s-d)}}{\eta} = \frac{\sqrt{r_1 r_2}\cos\frac{\theta}{2}}{\eta} \tag{2}$$

Let e_0 denote the eccentricity of the transformed orbit. Then, the equation of the time-of-flight is given by

$$\frac{1}{2}\sqrt{\frac{\mu}{a^3}}t_f = E - e_0\sin E \tag{3}$$

which defines the relationship between the time-of-flight and the semi-major axes of the transfer orbits.

With detailed derivation omitted in this context, Eq. (3) can be converted into the following two equations.[4]

$$y^2 = \frac{m}{(\ell+x)(1+x)} \tag{4a}$$

$$y^3 - y^2 = m\frac{E-\sin E}{4\tan^3\frac{E}{2}} \tag{4b}$$

where ℓ and m are two constants defined by

$$\ell = \tan^2 \frac{\nu}{2}, \text{ and } m = \frac{\mu t_f^2}{8 r_{0p}^3}, \tag{5}$$

and $x = \tan^2 \frac{E}{2}$.

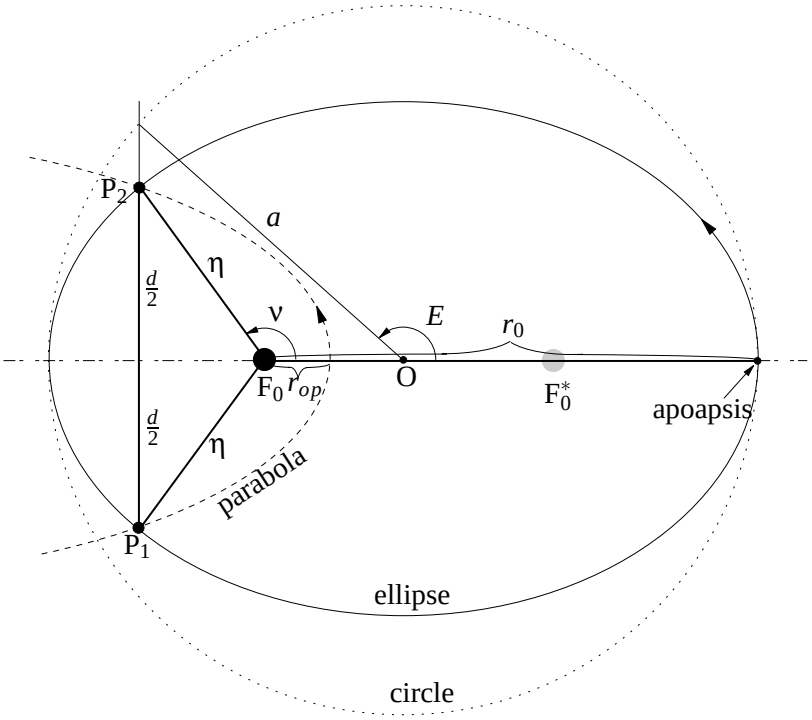

Figure 4: Transformation of the Lambert's problem - the P_1P_2 arc along the transformed orbit passes the apoapsis.

Equations (4) are Battin's formulation for the Lambert's problem. The variables y and x are to be solved using the method of successive substitutions.[3] The method starts with an initial guess $x = x_0$. Then E can be calculated from x. Next, y can be solved as the positive root of Eq. (4b). Then the newly-obtained y can be substituted into Eq. (4a) to solve for a new x. This process is repeated until y does not change within a given precision tolerance. This iterative process will be termed the *original successive substitution*. After y and x are obtained, the orbital elements can be easily calculated. The formulas for the semi-major axis and the semi-latus rectum of the original transfer orbit (not the transformed orbit) are given as [4]

$$a = \frac{ms(1+\lambda)^2}{8xy^2}, \text{ and } p = \frac{2r_1 r_2 y^2 (1+x)^2 \sin^2 \frac{\theta}{2}}{ms(1+\lambda)^2}. \tag{6}$$

Battin's formulation can also be used to calculate parabolic and hyperbolic transfer orbits. This

can be done by extending the definition of x to

$$x = \begin{cases} \tan^2 \frac{E}{2}, & \text{ellipse} \\ 0, & \text{parabola} \\ -\tanh^2 \frac{H_2 - H_1}{4}, & \text{hyperbola} \end{cases} \tag{7}$$

Therefore, in Battin's formulation, x ranges from -1 to $+\infty$.

Remark: For the case where the arc along the transformed orbit from P_1 to P_2 passes the apoapsis, the same formulation can be obtained. However, in this case, the definition of ν and E are no longer the true anomaly and eccentric anomaly of P_2 on the transformed orbit. The geometry of the transformation where the P_1P_2 arc passes the apoapsis is shown in Figure 4, along with the definition for ν and E. It can be seen that ν is the true anomaly of the point P_2 on the transformed orbit less π, and E is defined similarly. In addition, r_0 is defined as the radius of the apoapsis.

Battin's formulation, along with Gauss' formulation, is designed to calculate the transfer orbit where a space body traverses the arc from P_1 to P_2 along the transfer orbit only once. That is, the so-obtained transfer orbit is a 0-revolution transfer orbit. In the next section, we will study how Battin's formulation can be used to solve for multiple-revolution transfer orbits for the Lambert's problem.

EXTENSION OF BATTIN'S FORMULATION

With little additional effort following the derivation of Battin's formulation,[3] we can extend the formulation to accommodate N-revolution transfer orbits. The extended formulation can be written as the following two equations.

$$y^2 = \frac{m}{(\ell + x)(1 + x)} \tag{8a}$$

$$y^3 - y^2 = m \frac{N\pi + E - \sin E}{4 \tan^3 \frac{E}{2}}. \tag{8b}$$

Notice that when $N = 0$, Eqs. (8) are exactly the original formulation of Eqs. (4). In the following, for the convenience of presentation, we will use y_1 to denote the variable y in Eq. (8a) as a function of x, and y_2 to denote the variable y in Eq. (8b) as a function of x. Evidently, y_1 is a monotonically decreasing function of x. In Ref. 8, it is shown that y_2 is a monotonically decreasing function of x as well.

In the following, we will show how Eqs. (8) can be solved for x and y which determine the N-revolution transfer orbits. The two cases where $N = 0$ and $N > 0$ will be treated separately.

The Case When $N = 0$

When $N = 0$, there are three types of transfer orbits connecting the two points P_1 and P_2, depending on the transfer direction and transfer time. The three types of orbits are ellipse, parabola, and hyperbola. These transfer orbits are determined by the intersection of the functions y_1 and y_2. If the

intersection occurs when $-1 < x < 0$, then the transfer orbit is a hyperbola; if the intersection occurs when $x = 0$, then the transfer orbit is a parabola; and if the intersection occurs when $x > 0$, then the transfer orbit is an ellipse. In the following we use the elliptical transfer orbit as an example. That is, y_1 and y_2 intersects at $x > 0$.

From the geometry of the transformed orbit, it can be seen that the domain for E is $0 \le E < \pi$, so $x = \tan^2(E/2)$ is a monotonically increasing function of E in the domain of E. Furthermore, $x = 0$ when $E = 0$, and $x \to \infty$ when $E \to \pi$. Thus,

$$\lim_{x\to\infty} \frac{m}{(\ell+x)(1+x)} = 0, \text{ and } \lim_{x\to\infty} m\frac{E-\sin E}{4\tan^3\frac{E}{2}} = 0. \tag{9}$$

Therefore,

$$\lim_{x\to\infty} y_1 = 0, \text{ and } \lim_{x\to\infty} y_2 = 1. \tag{10}$$

In the meantime, it can be shown that when x approaches zero,

$$\lim_{x\to 0} \frac{m}{(\ell+x)(1+x)} = \frac{m}{\ell}, \text{ and } \lim_{x\to 0} m\frac{E-\sin E}{4\tan^3\frac{E}{2}} = \frac{m}{3}. \tag{11}$$

Let

$$y_{10} = \lim_{x\to 0} y_1, \text{ and } y_{20} = \lim_{x\to 0} y_2.$$

Then from Eq. (11), we get

$$y_{10} = \frac{m}{\ell}, \text{ and } y_{20}^3 - y_{20}^2 = \frac{m}{3}.$$

It has been shown in Ref. 8 that

$$y_{10} > y_{20}. \tag{12}$$

Therefore, Eqs. (12) and (10) imply that before the intersection, $y_1 > y_2$, and after the intersection, $y_1 < y_2$. These properties, combined with the fact that both y_1 and y_2 are monotonically decreasing functions, guarantee that at the intersection where $x = x^*$,

$$\left.\frac{dy_1}{dx}\right|_{x=x^*} \le \left.\frac{dy_2}{dx}\right|_{x=x^*}. \tag{13}$$

Consequently, the original successive substitution method for solving Eqs. (4a) and (4b) converges to x^*, with any initial guess $0 < x_0 < \infty$. This can be demonstrated by Figure 5 which shows an example of the plots of y_1 and y_2 as a function of x. This corresponds to a Lambert's problem where $r_1 = 1$, $r_2 = 2$, the transfer angle $\theta = 60^\circ$, and $t_f = 2.2$. In Figure 5, the intersection where $x = x^*$ is shown. It is clear that the relationship in Eq. (13) holds at x^*. The process of the original successive substitution is also demonstrated in the figure. The initial guess is at $x = x_0$. Then the new $x = x_1$ is such that $y_1(x_1) = y_2(x_0)$, and the new $x = x_2$ is such that $y_1(x_2) = y_2(x_1)$. After each iteration, x_{i+1} is closer to x^* than x_i. Eventually, the sequence $\{x_i\}$ converges to x^*.

The Case When $N > 0$

When $N > 0$, the only possible transfer orbits are ellipses. Recall that given a Lambert's problem, there are two N-revolution transfer orbits if $0 < N \le N_{\max}$. These two transfer orbits have different

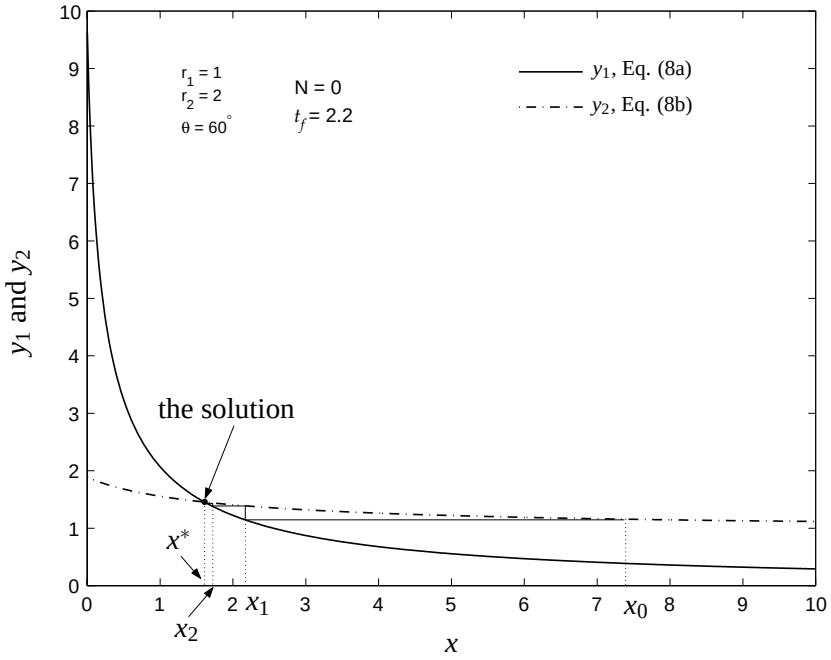

Figure 5: Plots of y_1 and y_2 vs. x for the original Battin's formulation ($N = 0$).

semi-major axes, and they may be all combinations of large-e and small-e transfer orbits. For example, a plot of t_f vs. a for a Lambert's problem is shown in Figure 6. This Lambert's problem is defined such that $r_1 = 1$, $r_2 = 2$, $\theta = 60^\circ$, and $t_f = 2.2$. It can be seen that there are two 1-revolution transfer orbits (points L and R) and one 0-revolution transfer orbit (point P), with the respective semi-major axes denoted by a_L, a_R, and a_P. However, the original successive substitution method using Battin's formulation only yields the transfer orbit at point P. The goal in this section is to explore the possibility of using Battin's formulation to solve for the transfer orbits at points L and R.

As an analogy to the scenario where there are two semi-major axes corresponding to one t_f in the time-of-flight equation (Eq. (1)) when $N \geq 1$, in Battin's formulation y_1 and y_2 have two intersections for $N \geq 1$. These two intersections determine the two transfer orbits. The plots of y_1 and y_2 of the above example with $N = 1$ is shown in Figure 7, where x_R^* and x_L^* denote the values of x at the intersections, with $x_R^* \leq x_L^*$. (At this point, we do not know which of the two N-revolution transfer orbits corresponds to x_R^* or x_L^*. The correspondence will be clarified later on.)

As have been shown above,

$$\lim_{x\to\infty} y_1 = 0, \quad \text{and} \quad \lim_{x\to\infty} y_2 = 1. \tag{14}$$

Thus, after the second intersection (at x_L^*), $y_2 > y_1$. In the meantime, it can be seen from Eqs. (8a) and (8b) that

$$\lim_{x\to 0} y_1 = \sqrt{\frac{m}{\ell}}, \quad \text{and} \quad \lim_{x\to 0} y_2 = \infty. \tag{15}$$

That is, before the first intersection (at x_R^*), we still have that $y_2 > y_1$. These two properties are evident in Figure 7. In addition, as shown in the figure, between the two intersections, $y_1 > y_2$.

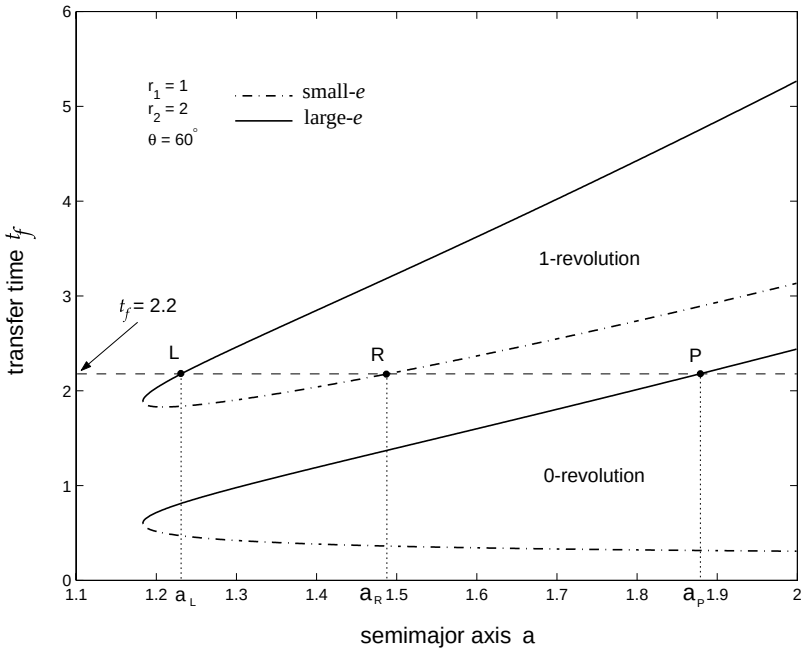

Figure 6: Plots of t_f vs. a.

These properties, combined with the fact that both y_1 and y_2 are monotonically decreasing functions, imply that at x_L^*,

$$\left.\frac{dy_1}{dx}\right|_{x=x_L^*} \leq \left.\frac{dy_2}{dx}\right|_{x=x_L^*}, \tag{16}$$

and at x_R^*,

$$\left.\frac{dy_1}{dx}\right|_{x=x_R^*} \geq \left.\frac{dy_2}{dx}\right|_{x=x_R^*}. \tag{17}$$

Therefore, it is clear that the original successive substitution procedure converges to x_L^* with any initial guess $x_0 > x_R^*$, as shown in Figure 7. However, it is also clear that the original successive substitution diverges from x_R^*, which implies that the original successive substitution can only be used to calculate one of the N-revolution transfer orbits.

However, it is evident from Figure 7 that if the order of the original successive substitution is reversed, then it converges to x_R^* with an initial guess of $x_0 < x_R^*$. That is, given an initial guess x_0, y_1 can be calculated from Eq. (8a). $y_2 = y_1$ is then substituted into Eq. (8b) to calculate the value of E which yields an x_1. x_1 is then used in Eq. (8a) again to calculate a new y_1. This process is repeated until y_1 does not vary within a given precision tolerance. This process is also demonstrated in Figure 7. We will denote this iterative process the *reversed successive substitution*.

Within each step of the reversed successive substitution procedure, E need to be calculated from Eq. (8b) for a given y_2. This will be addressed after the next subsection.

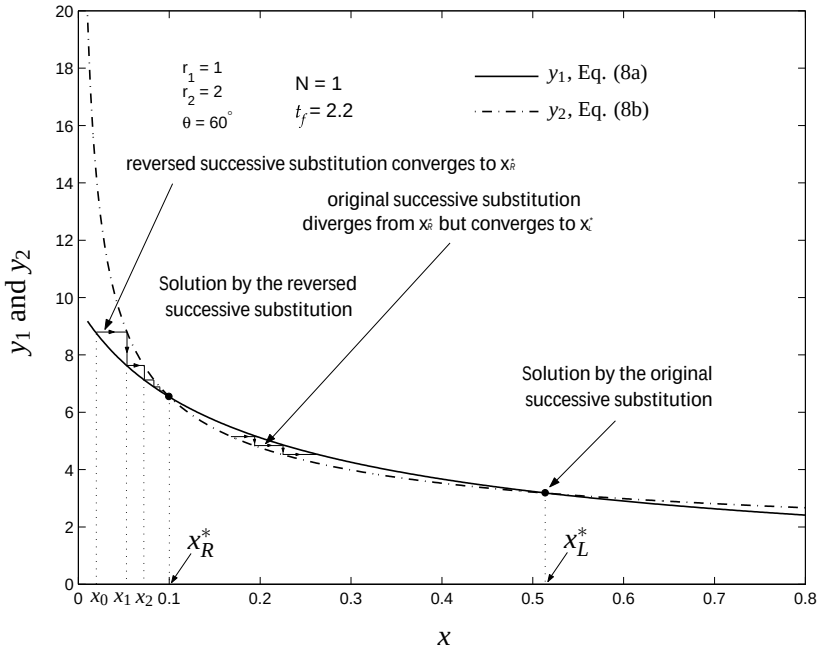

Figure 7: Plots of y_1 and y_2 vs. x for the extended Battin's formulation ($N > 0$).

Initial Guesses with Guaranteed Convergence

Notice that in reality, x_R^* and x_L^* are not known a priori. Thus, it is not possible to pick initial guesses less than x_L^* for the reversed successive substitution and initial guesses greater than x_R^* for the original successive substitution to converge. In practice, the following preprocessing procedure guarantees to provide initial guesses in the convergence region.

Whether it is x_R^* or x_L^* that needs to be solved, the starting point for x can be set as $x_0 = l = \tan^2 \nu/2$. First, let's consider the case when x_L^* needs to be solved. Starting with x_0, we can initiate the original successive substitution. We know that if $x_0 > x_R^*$, the iteration will converge to x_L^*, and if $x_0 < x_R^*$, the iteration will diverge. When the iteration diverges, the value of y_2 will eventually exceeds $\sqrt{m/l}$ which is the finite upper bound for y_1. Thus, at each step, we will monitor y_2. If at some step, $y_2 > \sqrt{m/l}$, we know that the iteration started from the divergent region for the original successive substitution ($x_0 \leq x_R^*$). In this case, the reversed successive substitution will be initiated with the starting point at x_0. This iteration will converge to x_R^*. Once x_R^* is obtained, the initial guess for obtaining x_L^* using the original successive substitution can be picked as any value larger than x_R^*. For example, it can be picked as $2x_R^*$.

Similar procedure can be followed if x_R^* needs to be solved. In this case, the reversed successive substitution is initiated with starting point at x_0. At each step, we monitor y_1. If at some step $y_1 < 1$, we know that x_0 is in the divergent region for the reversed successive substitution ($x_0 \geq x_L^*$). However, in this case, the original successive substitution can be used to calculate x_L^* starting from x_0. Once x_L^* is obtained, any value between 0 and x_L^* can be chosen as the initial guess for the reversed successive substitution to calculate x_R^*. For example, we can pick $x_L^*/2$ as the initial guess.

Calculating E in the Reversed Successive Substitution Method

As shown earlier, at each iteration in the reversed successive substitution method, given an intermediate value of y_2, E needs to be calculated from Eq. (8b). Since the right-hand side of Eq. (8b) is a transcendental function, a numerical algorithm is used to calculate E. In this paper, the Newton-Raphson iteration method is used.

To this end, let q be a constant defined as

$$q = \frac{4}{m}(y_2^3 - y_2^2),$$

and let $h(E)$ be a function defined as

$$h(E) = \frac{N\pi + E - \sin E}{\tan^3 \frac{E}{2}} - q. \tag{18}$$

Then, Eq. (8b) is equivalent to

$$h(E) = 0, \tag{19}$$

and the task is thus to solve E from Eq. (19).

The Newton-Raphson iteration method is the repetition of the following step. Suppose the value for E is given as E_i in the i^{th} step, then in the next step,

$$E_{i+1} = E_i - \frac{h(E_i)}{h'(E_i)}, \tag{20}$$

where $h'(E_i)$ denote the derivative of $h(E)$ with respect to E evaluated at E_i. In Ref. 8, it is shown that $h'(E) < 0$. Thus, the function $h(E)$ monotonically decreases with E, and there is only one value of E such that $h(E) = 0$. Let this value of E be denoted by E^*. It is also shown in Ref. 8 that $h''(E) \geq 0$. Thus, $h(E)$ is a convex function. Therefore, the convergence of the Newton-Raphson iteration method is guaranteed with an initial guess of E_0 such that $h(E_0) \geq 0$ (that is, $E_0 \leq E^*$), and the convergence is not guaranteed otherwise.

Since the solution E^* is not known a priori, it is not possible to pick an initial guess $E_0 \leq E^*$. in the following, a pre-processing of the initial guess is presented in order to arrive at an initial guess in the guaranteed convergence region.

Let the initial guess of E be E_0. First, we calculate $h(E_0)$. If $h(E_0) \geq 0$, then the Newton-Raphson iteration can be started. Otherwise, if $h(E_0) < 0$, we set $E_1 = E_0/2$, and use E_1 as the new initial guess, and repeat the pre-processing until we obtain E_i at the i^{th} step such that $h(E_i) \geq 0$. Then, E_i can be used as the initial guess for the Newton-Raphson iteration.

The idea of pre-processing an initial guess and the convergence of the Newton-Raphson iteration are demonstrated in Figure 8, where the plot of $h(E)$ is shown corresponding to the case when $q = 3$ and $N = 1$. In the figure, the initial guess E_0 is such that $h(E_0) < 0$ and the convergence is not guaranteed. Thus, the pre-processing is necessary which leads to $E_1 = E_0/2$. Since $h(E_1) > 0$, the convergence is guaranteed. The first a few steps of the Newton-Raphson iteration starting from E_1 are shown in the figure.

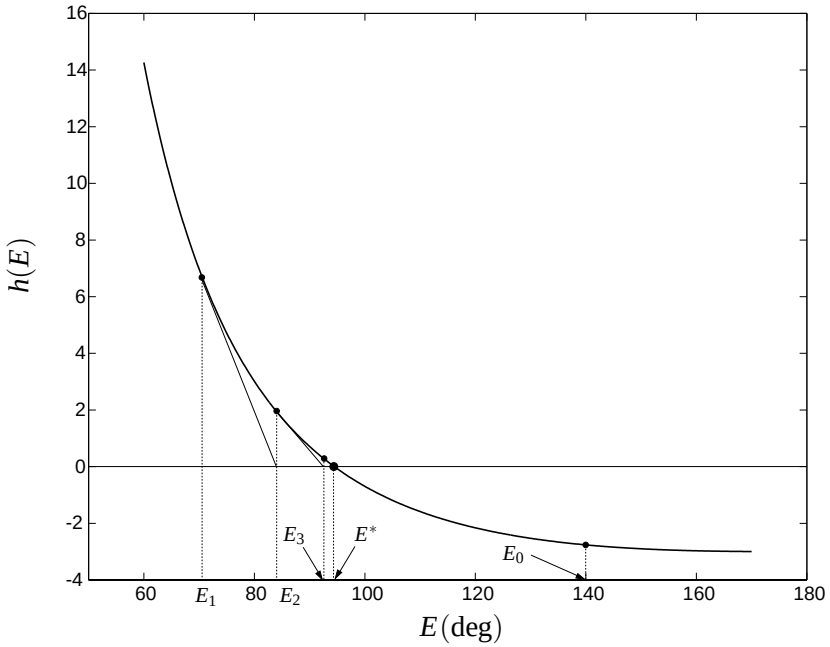

Figure 8: Demonstration of the procedure of obtaining E^* in the reversed successive substitution method.

DETERMINING THE TRANSFER ORBITS

Now that we have shown that the two N-revolution transfer orbits for $N \geq 1$ can be determined by the two intersections of y_1 and y_2, it remains to determine which of the two transfer orbits x_R^* or x_L^* determines. Recall that x_R^* can be obtained by the reversed successive substitution, x_L^* can be obtained by the original successive substitution, and $x_R^* \leq x_L^*$.

To this end, let a_L and a_R denote the semi-major axes of the two N-revolution transfer orbits, with $a_L \leq a_R$, as shown in Figure 6. Recall that there are two types of N-revolution transfer orbits, namely, the large-e and small-e transfer orbits. It has been shown in Ref. 8 that when $\theta \leq \pi$, a_R always determines a small-e transfer orbit, but a_L could correspond to either a small-e transfer orbit or a large-e transfer orbit, depending on the transfer time t_f. On the other hand, when $\theta > \pi$, a_R always determines a large-e transfer orbit, but a_L could correspond to either a large-e transfer orbit or a small-e transfer orbit, also depending on the transfer time t_f. Therefore, there are four cases to consider which are defined in Table 1. In the following, it will be shown from the geometry of the aforementioned orbit transformation that for each of the four cases, a_L corresponds to x_L^*, and a_R corresponds to x_R^*; i.e., x_L^* determines the N-revolution transfer orbit with the smaller semi-major axis, and x_R^* determines the N-revolution transfer orbit with the larger semi-major axis, regardless of whether the transfer orbits are large-e or small-e ones.

Case 1. In this case, the transfer angle $\theta \leq \pi$, and both a_L and a_R determine small-e transfer orbits.

The geometry of a small-e transfer orbit with $\theta \leq \pi$ and its transformed orbit is shown in

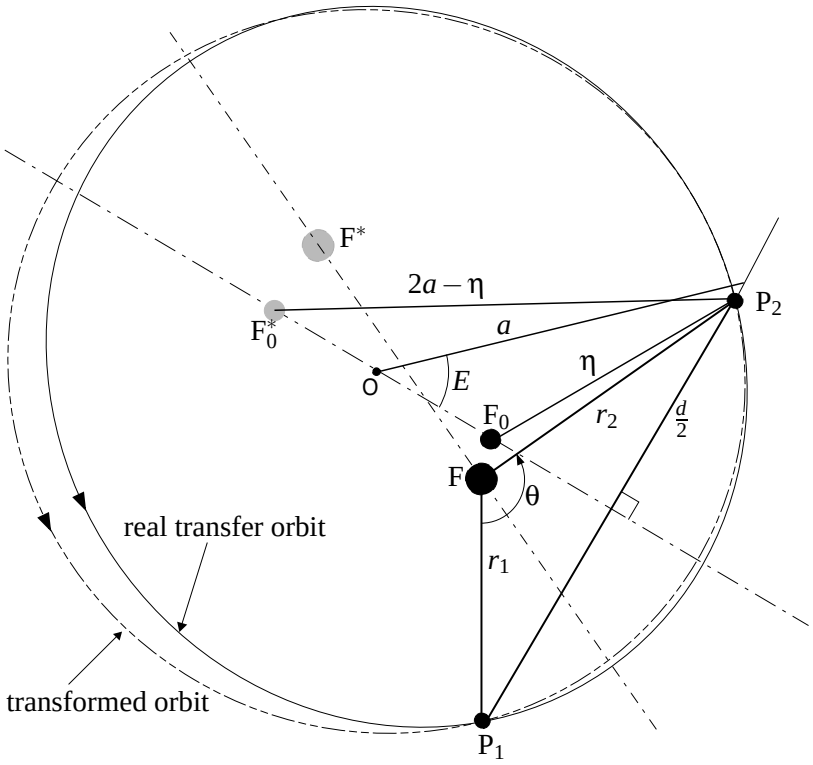

Figure 9: Transformation of a small-e transfer orbit with $\theta \leq \pi$.

Table 1: Definition of four different cases.

	θ	a_L corresponds to	a_R corresponds to
Case 1	$\leq \pi$	small-e	small-e
Case 2	$\leq \pi$	large-e	small-e
Case 3	$> \pi$	large-e	large-e
Case 4	$> \pi$	small-e	large-e

Figure 9. It can be seen from the geometry that

$$\cos E = \frac{\sqrt{\eta^2 - \left(\frac{d}{2}\right)^2} + \sqrt{(2a-\eta)^2 - \left(\frac{d}{2}\right)^2}}{2a} \tag{21}$$

In Ref. 8, it is shown that the right-hand side of Eq. (21) is a monotonically increasing function of a. Thus, E monotonically decreases with a. Recall that x is a monotonically increasing function of E because $x = \tan^2(E/2)$. Thus, x monotonically decreases as a increases. Since $a_L \leq a_R$ and $x_L^* \geq x_R^*$, we conclude that x_L^* corresponds to the transfer orbit with semi-major axis a_L, and x_R^* corresponds to the one with semi-major axis a_R.

Case 2. In this case, the transfer angle $\theta \leq \pi$, a_L determines a large-e transfer orbit, and a_R determines a small-e transfer orbit.

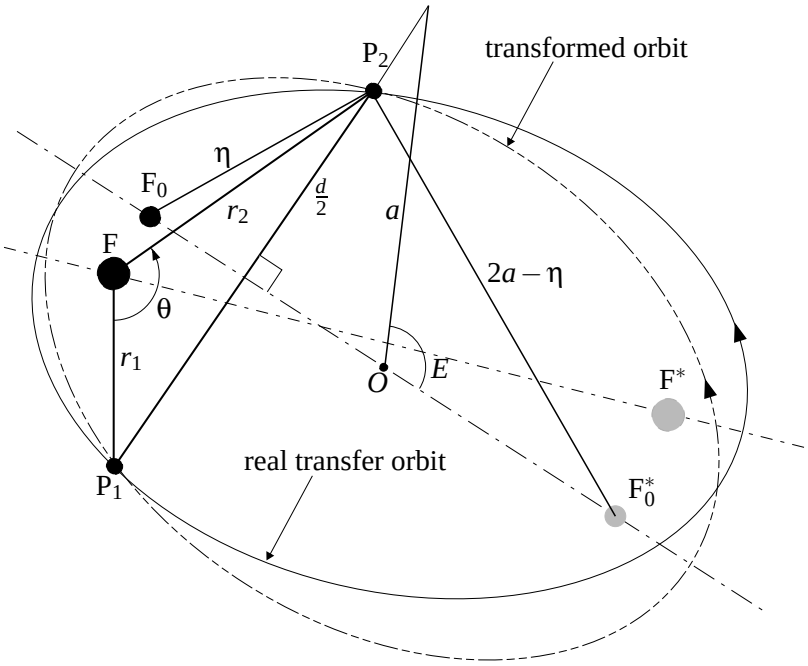

Figure 10: Transformation of a large-e transfer orbit with $\theta \leq \pi$.

The geometry of a large-e transfer orbit with $\theta \leq \pi$ and its transformed orbit is shown in Figure 10. It can be seen from the geometry that

$$\cos E = \frac{\sqrt{\eta^2 - \left(\frac{d}{2}\right)^2} - \sqrt{(2a-\eta)^2 - \left(\frac{d}{2}\right)^2}}{2a} \tag{22}$$

Let E_L be the eccentric anomaly of the transformed orbit corresponding to a_L, and E_R be the eccentric anomaly of the one corresponding to a_R. Then $\cos E_L$ is given by Eq. (22), and since a_R determines a small-e transfer orbit, $\cos E_R$ is given in Eq. (21). Hence,

$$\begin{aligned}
\cos E_L &= \frac{\sqrt{\eta^2 - \left(\frac{d}{2}\right)^2} - \sqrt{(2a_L-\eta)^2 - \left(\frac{d}{2}\right)^2}}{2a_L} \\
&\leq \frac{\sqrt{\eta^2 - \left(\frac{d}{2}\right)^2} + \sqrt{(2a_L-\eta)^2 - \left(\frac{d}{2}\right)^2}}{2a_L} \\
&\leq \frac{\sqrt{\eta^2 - \left(\frac{d}{2}\right)^2} + \sqrt{(2a_R-\eta)^2 - \left(\frac{d}{2}\right)^2}}{2a_R} \\
&= \cos E_R,
\end{aligned} \tag{23}$$

where the last inequality is because of the fact that the right-hand side of Eq. (21) is a monotonically increasing function of a. Thus, we have $E_L \geq E_R$. Because $x = \tan^2 \frac{E}{2}$, we can conclude that the value of x^* corresponding to the transfer orbit with semi-major axis a_L is larger than that corresponding to the transfer orbit with semi-major axis a_R. Therefore, since $x_L^* \geq x_R^*$, x_L^* corresponds to a_L, and x_R^* corresponds to a_R.

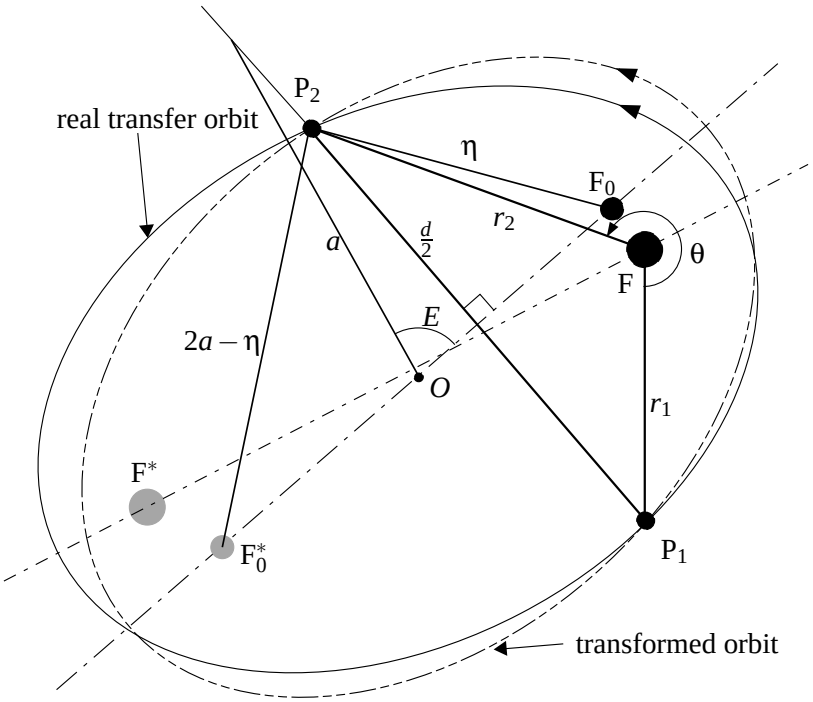

Figure 11: Transformation of a large-e transfer orbit with $\theta > \pi$.

Case 3. In this case, the transfer angle $\theta > \pi$, and both a_L and a_R determines large-e transfer orbits.

Figure 11 shows the geometry of a large-e transfer orbit with $\theta > \pi$ and its transformed orbit. It can be seen from the geometry that

$$\cos E = \frac{\sqrt{(2a-\eta)^2 - \left(\frac{d}{2}\right)^2} - \sqrt{\eta^2 - \left(\frac{d}{2}\right)^2}}{2a} \tag{24}$$

In Ref. 8, it is shown that the right-hand side of Eq. (24) is a monotonically increasing function of a. Thus, E monotonically decreases with a. Thus, x monotonically decreases as a increases because $x = \tan^2 \frac{E}{2}$. Therefore, since $a_L \leq a_R$ and $x_L^* \geq x_R^*$, we conclude that x_L^* corresponds to a_L, and x_R^* corresponds to a_R.

Case 4. In this case, the transfer angle $\theta > \pi$, a_L determines a small-e transfer orbit, and a_R determines a large-e transfer orbit.

Figure 12 shows the geometry of a small-e transfer orbit with $\theta > \pi$ and its transformed orbit. It can be seen from the geometry that

$$\cos E = \frac{-\sqrt{(2a-\eta)^2 - \left(\frac{d}{2}\right)^2} - \sqrt{\eta^2 - \left(\frac{d}{2}\right)^2}}{2a} \tag{25}$$

Let E_L be the eccentric anomaly of the transfer orbit determined by a_L, and let E_R be the eccentric anomaly of the one determined by a_R. In this case, $\cos E_L$ is given by Eq. (25), and

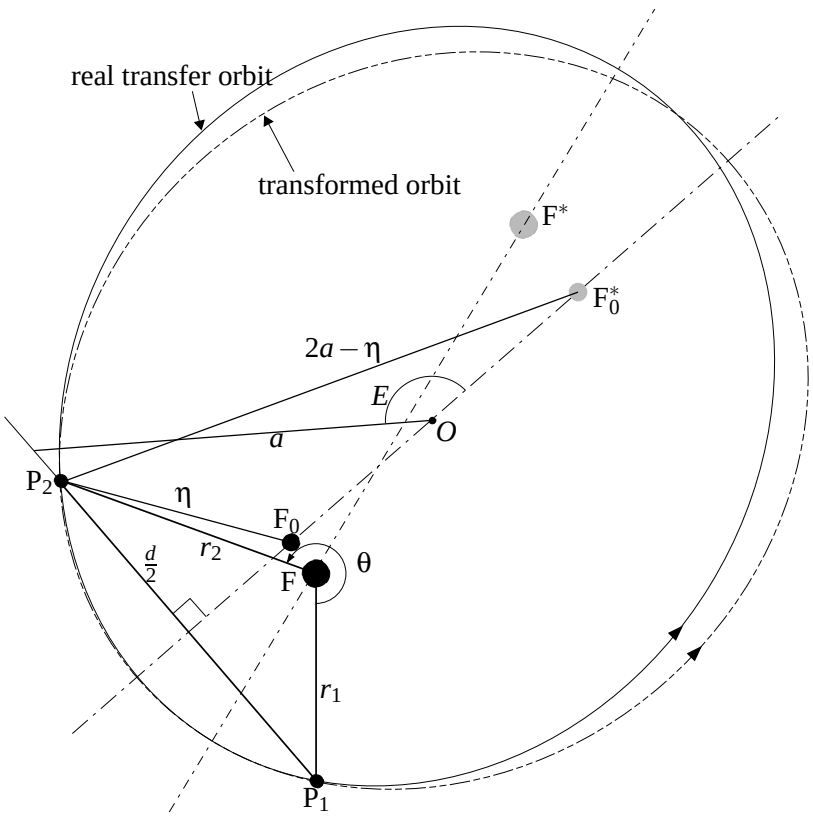

Figure 12: Transformation of a small-e transfer orbit with $\theta > \pi$.

$\cos E_R$ is given by Eq. (24). Hence, we have

$$\begin{aligned}\cos E_L &= \frac{-\sqrt{(2a_L-\eta)^2-\left(\frac{d}{2}\right)^2}-\sqrt{\eta^2-\left(\frac{d}{2}\right)^2}}{2a_L} \\ &\le \frac{\sqrt{(2a_L-\eta)^2-\left(\frac{d}{2}\right)^2}-\sqrt{\eta^2-\left(\frac{d}{2}\right)^2}}{2a_L} \\ &\le \frac{\sqrt{(2a_R-\eta)^2-\left(\frac{d}{2}\right)^2}-\sqrt{\eta^2-\left(\frac{d}{2}\right)^2}}{2a_R} \\ &= \cos E_R,\end{aligned} \tag{26}$$

where the last inequality is from the fact that the right-hand side of Eq. (24) is a monotonically increasing function of a and $a_L \le a_R$. Thus, $E_L \ge E_R$, which implies that a_L corresponds to a larger value of x than a_R does. Therefore, we again conclude that x_L^* corresponds to a_L, and x_R^* corresponds to a_R.

Therefore, we have shown the original successive substitution which determines the larger x^* yields the N-revolution transfer orbit with the smaller semi-major axis, while the reversed successive substitution which determines the smaller x^* yields the N-revolution transfer orbit with the larger semi-major axis.

CONCLUSION

In this paper, Battin's formulation is extended to calculate the multiple-revolution Lambert's solution. When solving for a 0-revolution transfer orbit, Battin's original successive substitution procedure converges with any initial guess of $-1 < x_0 < \infty$. For the two N-revolution transfer orbits (with $N \geq 1$), Battin's original successive substitution procedure converges to the one with the smaller semi-major axis. The initial guess for x has to be large enough, namely, it has to be greater than x_R^*. The reversed successive substitution procedure can be used to compute the transfer orbit with the larger semi-major axis. The initial guess for x has to be small enough, namely, it has to be smaller than x_L^*. A procedure is also proposed to generate initial guesses with which the convergence is guaranteed.

References

[1] R. R. Bate, D. D. Mueller, and J. E. White. *Fundamentals of Astrodynamics*. Dover Publications, Inc., New York, 1971.

[2] J. M. A. Danby. *Fundamentals of Celestial Mechanics*. Willmann-Bell, Richmond, VA, 2 edition, 1988.

[3] R. H. Battin. An elegant lambert algorithm. *Journal of Guidance, Control, and Dynamics*, 7(6):662 –670, 1986.

[4] R. H. Battin. *An Introduction to the Mathematics and Methods of Astrodynamics*. AIAA Education Series, AIAA, Reston, VA, 1999.

[5] J. E. Prussing. A class of optimal two-impulse rendezvous using multiple-revolution Lambert solutions. In *Advances in the Astronautical Sciences*, volume 106, pages 17–39, San Diego, CA, 2000. Univelt, Inc.

[6] R. H. Battin, T. J. Fill, and S. W. Shepperd. A new transformation invariant in the orbital boundary-value problems. *Journal of Guidance, Control, and Dynamics*, 1(1):50–55, 1978.

[7] H. Shen and P. Tsiotras. Optimal two-impulse rendezvous between two circular orbits using multiple revolution Lambert's solutions. In *AIAA Guidance, Navigation, and Control Conference, Monterey, CA*, Aug. 5-8, 2002. AIAA-2002-4844.

[8] H. Shen. *Optimal Scheduling For Satellite Refuelling In Circular Orbits*. PhD thesis, Georgia Institute of Technology, 2003.